Towards Durability Estimation of Bioprosthetic Heart Valves Via Motion Symmetry Analysis

Maryam Alizadeh, Melissa Cote, and Alexandra Branzan Albu
Electrical and Computer Engineering, University of Victoria
Victoria, BC, Canada
{alizadeh,mcote,aalbu}@uvic.ca

Abstract

This paper addresses bioprosthetic heart valve (BHV) durability estimation via computer vision (CV)-based analyses of the visual symmetry of valve leaflet motion. BHVs are routinely implanted in patients suffering from valvular heart diseases. Valve designs are rigorously tested using cardiovascular equipment, but once implanted, more than 50% of BHVs encounter a structural failure within 15 years. We investigate the correlation between the visual dynamic symmetry of BHV leaflets and the functional symmetry of the valves. We hypothesize that an asymmetry in the valve leaflet motion will generate an asymmetry in the flow patterns, resulting in added local stress and forces on some of the leaflets, which can accelerate the failure of the valve. We propose two different pair-wise leaflet symmetry scores based on the diagonals of orthogonal projection matrices (DOPM) and on dynamic time warping (DTW), computed from videos recorded during pulsatile flow tests. We compare the symmetry score profiles with those of fluid dynamic parameters (velocity and vorticity values) at the leaflet borders, obtained from valve-specific numerical simulations. Experiments on four cases that include three different tricuspid BHVs yielded promising results, with the DTW scores showing a good coherence with respect to the simulations. With a link between visual and functional symmetries established, this approach paves the way towards BHV durability estimation using CV techniques.

1. Introduction

1.1. Context

Valve replacement procedures are routinely used in clinical settings to replace defective native heart valves in patients suffering from valvular heart disease, with around 300,000 procedures performed yearly worldwide [24]. Between 40 and 60 percent of these procedures involve bioprosthetic heart valves (BHVs), which are produced using
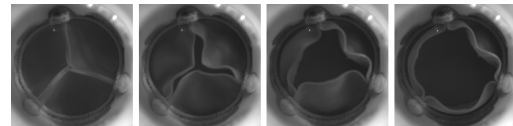
Figure 1. Sample frames of a tricuspid BHV from a high-quality *in vitro* pulsatile flow test video, at different moments of the cardiac cycle (opening phase shown here).

glutaraldehyde-fixed animal (bovine or porcine) tissue [37]. Compared to mechanical valves, BHVs tend to have a more natural behavior [23], do not present thrombogenicity complications and circumvent the problem of anti-coagulation medications [20], and can be delivered using minimally-invasive techniques [19]. However, they are not as mechanically robust and exhibit limited durability in younger patients, particularly those younger than 60 years [19]. In fact, more than 50% of BHVs encounter a structural failure within 15 years post-implantation [31], with tears (and calcification) being responsible for a majority of the failures [31, 32]. Tears on the valve leaflets mostly happen in areas under highly localized mechanical forces [32].

This paper aims to investigate the correlation between the visual symmetry of BHVs in motion and their functional symmetry performance. The goal is to pave the way for utilizing computer vision (CV) techniques to estimate the durability of BHVs. We focus on tricuspid BHV designs, which contain three symmetric leaflets. Figure 1 shows example frames extracted from high-quality videos taken during *in vitro* pulsatile flow tests, at various moments in the cardiac cycle. A cardiac cycle includes the opening, open, closing, and closed phases. Pulsatile flow tests are typically carried out during the valve design process to assess its performance via mechanical simulations of the cardiac flow (see Sec. 3.1). In addition to allow for the extraction of measurements related to the hydraulic and fluid dynamic parameters of the valve, these mechanical tests are typically coupled with high-speed digital cameras that record the valve's opening and closing patterns with great detail, opening up the way for visual inspections and thus CV-based analyses

of the valve behavior [2]. Here, we analyze the symmetry of the valve's opening and closing patterns at the leaflet level. We aim to show that an asymmetry in the motion of each leaflet, compared to that of other leaflets, leads to differences in stress and forces on each leaflet (increased in some cases), which can affect the durability of the valve.

1.2. Related Works

In vitro tests are typically carried out prior to the implantation of BHVs within the human body to assess the performance of the designs and potential modes of failures. Such assessments can be categorized into numerical and mechanical simulations. On one hand, numerical simulations are of great help to understand the dynamics involved in valve functions (e.g. [6]) and are most useful when experimenting with various designs. On the other hand, mechanical simulations, such as pulsatile flow tests, physically submit the actual BHVs to realistic physiological settings, and are most useful when the valve designs are set and the valves are constructed. Mechanical simulations and the *in vitro* measurements of hydraulic and fluid dynamic parameters provide effective indications of BHV performance [12].

As this paper focuses on CV applications, a review of the literature on numerical simulations of BHVs is out of the paper's scope. In this section, we first focus on valve assessment using visual data acquired with high-speed cameras during mechanical simulations such as pulsatile flow tests, and second on symmetry analysis in visual data.

1.2.1 Heart Valve Assessment

Methods for valve assessment using visual data from high-speed videos can be divided into early works, which made use of external markers and particles to help process the videos, and more recent works, which forgo the use of such external aids and focus instead on the pixel intensities in the video frames. Here we review the latter.

Methods based exclusively on the valves' original pixel intensities include digital kymography, thresholding, and deformable models. Digital kymograms, which consist of image lines projected along a time axis, have been part of several works by Kondruweit *et al.* [17, 18]. One downside is that they focus only on a small region of the valve. Hahn *et al.* [13] tested three variations of thresholding-based methods to segment the orifice region of tricuspid valves and assess the leaflet fluttering: manual, Otsu's, and finite mixture model-based thresholding. As it is difficult to achieve a homogeneous background against which to project the valve orifice [7], thresholding only-based methods typically fail in the presence of non-homogeneous orifices. In part to address this non-homogeneity issue, many works have proposed deformable models, such as active contours (snakes) and level sets, to extract the valve orifice region, the evolution of the valve orifice region over time

being a standard evaluation metric of valve designs [2]. In a slightly different context, investigating valve movements via endoscopic high-speed recordings of native pig heart valves in an *ex vivo* setting, Wittenberg *et al.* [36] used manually initialized snakes and local constraints manually applied to the leaflets' anchor points to extract the valve orifice region. In a similar setup, Kondruweit *et al.* [17] analyzed the effective orifice region through a combination of digital kymograms and snakes, both manually initialized. In an *in vitro* experimental setup closer to our own (see Sec. 3.1), and in an effort to automate the process, Condurache *et al.* [7] compared automatic thresholding, similar to that of [13], with snakes that included automatically added leaflet anchor points-based attractors to better capture the leaflet boundaries. The authors also tackled the automatic analysis of leaflet fluttering [8], detected from leaflet curves as a high frequency signal superimposed on the portion of the curve corresponding to the open phase of the cardiac cycle. Utilizing snakes and a separate curve expansion scheme, Alizadeh *et al.* [1] detected the leaflet free edges as opposed to the valve orifice region, which more accurately represent the leaflet motion. In a follow-up paper [2], the authors increased the detection accuracy utilizing a combination of snakes, thresholding, and an improved expansion scheme. Focusing on the valve orifice region itself, Burden *et al.* [4] integrated a probabilistic motion boundary model into a distance regularized level set evolution formulation. This model allowed them to constrain the evolution domain using valve-specific motion data.

As there is no literature on symmetry assessment for BHV performance evaluation, below we review relevant works on visual symmetry analysis from other applications.

1.2.2 Symmetry Assessment

Symmetry, in the general sense, expresses the notion that a structure is made from multiple copies of the same smaller unit. More formally, symmetry is examined via the effect of transformations on the structure in a certain space such that its sub-parts map to each other [21]. In the 2D Euclidean space, there are four types of elemental symmetries: reflection, rotation, translation, and glide reflection. In CV, research on symmetry has mostly focused on reflection symmetry, with an increasing awareness of the entire symmetry spectrum [21]. Techniques for measuring symmetry in visual data can be divided into global and local; local techniques can be further divided into area- and feature-based.

Global techniques are generally based on applying certain types of transforms to search for symmetry axes [34]. For instance, Derrode and Ghorbel [9] used the Fourier–Mellin transform for symmetry detection in gray-level objects, Shen *et al.* [30] developed a unified method for detecting reflection and rotation symmetry in 2D images based on generalized complex moments, and Kondra

et al. [16] proposed multi-scale kernel operators for reflection and rotation symmetry detection in real-world scene images. Global techniques, which consider information derived from entire images, can characterize all potential symmetries but are typically less efficient than local techniques.

Area-based local techniques are among the easiest ones to implement but do not consider shape-related information. In general terms, maximal symmetry happens when two areas completely match, for instance via convolution or area ratio computations. Most area-based works come from medical image registration applications (e.g. [25, 28]).

Feature-based local techniques consider higher-level information embedded in the shape, contour, and/or other key features of images. They use feature descriptors and rely on information extracted from pixel intensity, pixel intensity changes, contour shapes, etc. In one of the early papers, Reisfeld and Yehezkel [27] proposed to use gradient information to detect facial features via generalized symmetry. Their symmetry score compared the gradient intensity and orientation between two points. Keypoint-based symmetry analysis methods such as those based on the scale invariant feature transform (SIFT) descriptor [5, 22, 26] may have difficulties in capturing structure-based patterns mostly supported by edges and contours [3]. Atadjanov and Lee [3] focused on edges and proposed a scale invariant structure feature that describes points on extremum curvature along edges to detect reflection symmetry. Wang *et al.* [34] established the correspondence of locally affine invariant edge-based features to detect single and multiple reflection symmetry axes in synthetic and real-world images. Their approach relied on diagonals of orthogonal projection matrices (DOPM) as contour descriptors for contour matching, invariant to the full set of affine transformations [33].

Works on reflection symmetry typically try to find the symmetry axis knowing or assuming that the data are symmetric, by looking at reflected parts. We use the concept of symmetry differently: we know where the symmetry axis is, and want to quantify the "degree" of symmetry.

1.3. Contributions

Our contributions are three-fold:

1. From a theoretical viewpoint, we propose to utilize visual symmetry information derived from the shape of pair-wise valve leaflet motions to perform BHV analyses via two different symmetry scores: the first one is based on the DOPM [33] and the second one on dynamic time warping (DTW) [11].
2. From an experimental viewpoint, we show, via numerical simulations, that the CV-based evaluation of symmetry, in particular the one using DTW, is coherent with the functional symmetry of the valves.
3. From a practical viewpoint, we pave the way towards BHV durability estimation using CV methods, having
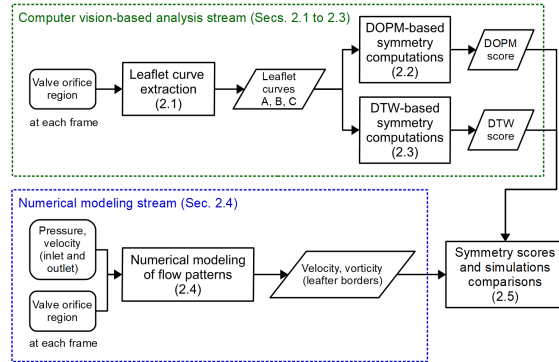
Figure 2. Flowchart of the proposed method. The three leaflet curves of the tricuspid valves are extracted from video data (valve orifice region) and their pair-wise symmetry is analyzed via two different scores (DOPM and DTW). The score profiles are then compared to the results of numerical simulations to validate the link between visual symmetry and functional symmetry.

> linked visual and functional symmetry to enable the indirect evaluation of the flow pattern and turbulence influencing the durability of BHVs.

We understand this paper to be the first to 1) propose a link between visual and functional symmetry of BHV leaflets, 2) utilize numerical simulations with CV-based techniques to validate this hypothesis, and 3) utilize DTW for symmetry analysis. Visual symmetry refers to reflection symmetry (see [35]) between two leaflets A and B, where there exists a line passing through the common anchor point of the two leaflets such that the border of A is the mirror image of the border of B. Functional symmetry refers to an agreement in the physical values found at the border of two leaflets A and B, in particular in velocity and vorticity.

2. Proposed Method

Figure 2 shows the proposed method's flowchart, divided into two streams: CV-based analysis (top), and numerical modeling (bottom), converging in the end to show the correlation between visual and functional symmetry. For the CV stream, the contour of the valve orifice region, obtained from high-quality videos recorded during *in vitro* pulsatile flow tests and input to the system for each frame, is divided into three leaflet curves. The leaflet curves are then used for pair-wise motion symmetry analysis via the computation of two symmetry scores: DOPM and DTW. For the numerical modeling stream, numerical simulations of the flow patterns during the cardiac cycle are conducted to estimate the amount of stress and forces on the leaflets. The simulations make use of the valve orifice region and of measured velocity and pressure data obtained during *in vitro* pulsatile flow tests as input, and output velocity and vorticity values at the leaflet borders. Finally, the symmetry scores are compared with the simulation results to assess their similarity.
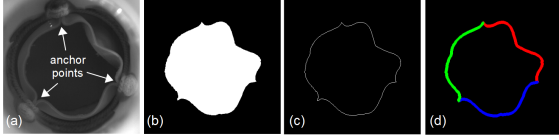
Figure 3. Leaflet curve extraction. Original frame (a), valve orifice region mask (b), contour of the valve orifice region (c), and three extracted leaflet curves shown in green, red, and blue (d).

2.1. Leaflet Curve Extraction

To evaluate the existing symmetry between the leaflets of a BHV, we consider three pair-wise leaflet groups, which yield three cases of bilateral symmetry. This allows us to analyze the valve symmetry at the leaflet level and determine which leaflet, if any, causes an asymmetry in the valve orifice region during the cardiac cycle. This process is carried out for each frame of the pulsatile flow test video.

The binary mask of the valve orifice region is used as input to the leaflet curve extraction step (Figure 3b). This mask can be obtained via one of the valve orifice segmentation methods from the literature (e.g. [2, 4, 8]), or from ground truth data. We selected the latter option, using the semi-automatic ground-truthing approach of [2], to discard any valve orifice segmentation error that would impact the evaluation of our method. The contour of the valve orifice region (Figure 3c) corresponds to the leaflet boundaries. For symmetry analysis purposes, we need to identify which part of the contour corresponds to each of the three leaflets. We base this split on the location of the anchor points (Figure 3a) and the valve center, found as follows. To obtain a rough skeleton representation of the valve orifice, dilation and thinning are applied to the input mask from one of the first few frames of the opening phase. The linear Hough transform is then applied on the skeleton representation to find three centerlines, at approximately 120 deg from each other. The intersection of the centerlines gives us the valve center. As the valve diameter d is a known parameter, the valve circular outline (stent) is readily found with respect to the valve center. The centerlines are then extended from their end point closest to the circular outline and the three anchor points are found as the intersection of the centerlines with the circular outline. The contour is then split into three segments (leaflet curves) at the anchor points (Figure 3d). The line passing through the anchor point common to two leaflets and the valve center is used later on as the symmetry axis for bilateral symmetry analysis, and also for reflecting a leaflet curve and superimposing it on the other leaflet curves. The three leaflet curves are used to calculate the two symmetry scores as explained next.

2.2. DOPM-Based Symmetry

DOPM, reviewed in Sec. 1.2.2, has been used for contour matching [33] and for the detection of reflection symme-

try [34]. Using edge information, it relies on the curvature of two curves to evaluate their symmetry. It has been shown to be affine invariant and appropriate in the context of capturing structure-based patterns, which is desirable here.

DOPM is based on the concept of edge fragments, or leaflet curve fragments in our case. An edge fragment E_i on a curve is defined around an edge point $\boldsymbol{X}_i$ on the curve:

$$E_i = [\boldsymbol{X}_{i-n}, ..., \boldsymbol{X}_i, ..., \boldsymbol{X}_{i+n}]^T, \qquad (1)$$

where $X_i^T = [x_i, y_i]$ represents the edge point Cartesian coordinates. The edge fragment is thus the n-neighborhood of the edge point (we use $n = 10$). The centerized configuration matrix $\breve{E}_i$ is introduced to move this edge fragment E_i to the origin and remove translation effects:

$$\breve{E}_i = (I - \frac{1}{n}\mathbf{1}_n\mathbf{1}_n^T)E_i, \qquad (2)$$

where I is the identity matrix and $\mathbf{1}_n \coloneqq [1, ..., 1]^T \in \mathbb{R}^n$. As its name suggests, the DOPM descriptor W_{E_i} is then computed from Eq. (2) as the diagonal of the orthogonal projection matrix:

$$W_{E_i} = \mathrm{diag}(\Pi_{\breve{E}_i})^{\frac{1}{2}}, \qquad (3)$$

where $\Pi_{\breve{E}_i}$ is the orthogonal projection matrix on the range space of $\breve{E}_i$. We define the following similarity metric γ between the edge fragments of two leaflet curves A and B:

$$\gamma(\breve{E}_i^A, \breve{E}_i^B) \coloneqq \|W_{E_i^A} - W_{E_i^B}\|_1, \qquad (4)$$

where $\|\cdot\|_1$ denotes the 1-norm of the subtracted vector. γ is calculated for all the edge points on the leaflet curve A and their corresponding match on the leaflet curve B. The final DOPM score is obtained as the average of all γ values:

$$\mathrm{DOPM\ score} = \frac{1}{p}\sum_{i=1}^{p}\gamma(\breve{E}_i^A, \breve{E}_i^B), \qquad (5)$$

where p is the length of the smaller of the two leaflet curves A and B. One should note that the smaller the DOPM score value, the higher the symmetry. Large values indicate the presence of asymmetry.

In [34], as symmetry is assumed and must be located, the two curves involved have the same length. In our case, symmetry is not assumed and the leaflet curves can be of different lengths, since they are the product of a 2D projection on the image plane of their 3D shape. The process for finding corresponding edge points from two leaflet curves is thus not trivial. We propose the following matching scheme. Let us assume that leaflet curve A is shorter than leaflet curve B. All points from A will make it to the final list of matched points, whereas some points from B will be discarded. The process starts with the first point on A, for which the DOPM descriptor (Eq. (3)) is calculated. The DOPM descriptors
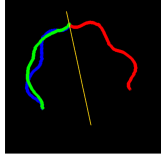
Figure 4. Superimposing the leaflet curves for the DTW score. The green and red leaflet curves are under examination for symmetry assessment, and the blue curve shows the reflection of the red curve about the symmetry axis (yellow line).

are then calculated for the first n points (search neighborhood) on B. The point on B that yields the lowest γ value is considered as the best match for the first point on A. To preserve monotonicity, the matched point on B is considered as the point on the lower end of the search neighborhood for the next point. The DOPM score is computed for all frames of the cardiac cycle.

2.3. DTW-Based Symmetry

We propose to adapt the DTW as a second way to measure the reflective symmetry between two leaflet curves via a DTW score. DTW was developed as an algorithm for measuring the similarity between two temporal sequences, first used in the context of speech recognition [10]. As a similarity measure between sequences of points in a metric space, it has since been massively used in various fields of computer science and computational biology [11].

DTW finds the optimal match between two curves that yields the minimum summation of the absolute distance between corresponding points. Let us consider two curves (A and B) represented by the following:

$$A = (a_1, a_2, ..., a_n), B = (b_1, b_2, ..., b_m), \quad (6)$$

where a_i and $b_j = [x_i y_i]^T$ are the coordinates of the ith and j^{th} points on A and B, and n and m are the length of A and B, respectively. The DTW algorithm finds all possible alignment paths between points a_i and b_j which satisfy the following conditions: 1) Boundary condition: the first and last points of the curves should be the first and last points of the aligned sequence, i.e. a_1 and b_1 should be paired together as well as a_n and b_m. This, however, does not need to be their only match. 2) Monotonicity condition: the order of the points should be preserved, i.e. the order of the aligned indices is never descending. The alignment path with the minimum summation of the absolute pairwise distances is considered as the optimal alignment path. The minimum summation value is used as the DTW score. Since a higher distance implies a larger discrepancy between curves, the smaller the DTW score value, the higher the symmetry. To calculate the DTW score between two leaflet curves in a way that takes into account reflection symmetry, we first need to superimpose them. The first leaflet is thus reflected about the symmetry axis of the leaflets' pair, which is the

line passing through the common anchor point of the leaflets and the valve center. Figure 4 shows an example of the two leaflets (red and green) in one leaflet pair, their symmetry axis (yellow) and the reflected curve (blue) of the first leaflet. The DTW score between the two superimposed leaflet curves is calculated for each pair of leaflets and for all frames of the cardiac cycle.

2.4. Numerical Modeling of Flow Patterns

We utilize a numerical model and conduct simulations of the cardiac cycle to investigate the correlation between the visual symmetry (analyzed via the DOPM and DTW scores) and the functional symmetry (agreement in the velocity and vorticity values found at the border of two leaflets). In the absence of a measured flow pattern at the leaflet borders, the goal is to confirm the possible impact of the valve opening asymmetries on the flow irregularities, which can lead to valve failure in the long term. The simulated values are observed throughout one cycle and their evolution is compared with that of the symmetry scores.

Our model is based on an open-source multi-physics solver (MPARS) [15, 29]. We selected this solver since in addition to being free and open-source, its mesh-free Lagrangian numerical method lends itself to a natural handling of highly dynamic irregular immersed boundaries (here the heart valve), which are challenging for conventional mesh-based Eulerian methods [29]. The numerical model solves the conservation of mass (continuity) and momentum (Navier–Stokes) equations for incompressible flow in a Lagrangian framework:

$$\begin{cases} \frac{D\rho}{Dt} + \rho(\nabla \cdot \boldsymbol{u}) = 0 & \text{Continuity} \\ \rho\frac{D\boldsymbol{u}}{Dt} = -\nabla p + \mu\nabla^2\boldsymbol{u} + \boldsymbol{g} & \text{Momentum} \end{cases} \quad (7)$$

where ρ is the fluid density, $\boldsymbol{u} : (u, v, w)$ is the fluid velocity vector in Cartesian coordinates $\boldsymbol{x} : (x, y, z)$, p is the pressure, μ is the fluid dynamic viscosity, and $\boldsymbol{g}$ is the gravity vector. The numerical methods represent the computational domain with a set of free-to-move particles (nodes) over which Eqs. (7) are integrated (discretized) using a moving particle semi-implicit technique [29]. The time integration is via a predictor-corrector algorithm, and turbulence is modeled using a large eddy simulation model [29].

The simulations make use of pressure and velocity data measured at the inlet and outlet during *in vitro* pulsatile flow tests (as boundary conditions), and take into account the valve orifice region area available via the high-quality videos. They allow us to extract the velocity and vorticity fields at the leaflet borders. The velocity and vorticity give us the flow pattern (streamlines) as well as an indication of the shear stress, which are important cues of the functional symmetry. The setup details are given in Sec. 3.2.

2.5. Symmetry Scores and Simulations Comparisons

Once we have DOPM and DTW score profiles obtained with the CV stream and simulated velocity and vorticity profiles obtained with the numerical modeling stream over a cardiac cycle, we need to find out how much they correlate. This comparison cannot focus on the values themselves since they are not representing the same variables. Instead, we qualitatively investigate the overall trend and the location of the peaks in the graphs, and perform a quantitative difference-based comparison as follows. The mean value of the graphs is first removed from all values; this centers the graphs around a value of 0. The graphs are then normalized (rescaled to the range $[0, 1]$), and the root-mean-square error (RMSE) is calculated between the resulting graphs. Since there are three pairs of leaflets for each valve, there are three DOPM score profiles and three DTW score profiles that are each compared with the velocity and the vorticity profiles for each valve. This amounts to 12 comparisons per valve (6 scores x 2 simulated variables). One should note that the pair-wise velocity and vorticity profiles are computed as the absolute difference of the velocity and vorticity values at the border of the two leaflets involved.

3. Results and Discussion

3.1. Experimental Setup and Video Dataset

As there are no public BHV video datasets available, we have assembled our own. Our experimental setup to collect high-quality videos and pressure and velocity data involves tricupsid BHVs mounted in the Pulse Duplicator device from ViVitro Labs [14]. The device reconstructs the performance of native heart valves by simulating the physiological cardiac conditions and flow patterns. Figure 5 shows the schematics of the heart anatomy and the device side by side, with arrows indicating which parts of the heart are modeled by each chamber of the device. Pressure ports and flow measuring sensors, located before and after the valve, are used to collect data that are input to the numerical modeling. The device uses an anatomical model and a rigid anatomical aortic model with sinuses. The flow path is 28 mm in diameter. The inflow and outflow pressure transducers are located 65 mm and 85 mm from the midline of the valve, respectively. The midline of the electromagnetic flow probe is located 35 mm from the midline of the valve.

High-quality videos were captured during pulsatile tests and utilized as input to the CV processing. Videos were recorded for three different BHVs via a Photron SA3 high-speed digital camera, with a frame rate ranging from 250 to 1000 fps depending on the video, a shutter speed matching the frame rate, and a 300 ms test cycle, with resolutions between 400×400 and 1024×1024 pixels depending on the valve. Two of the BHVs (BHV-1 and BHV-2) were 25 mm
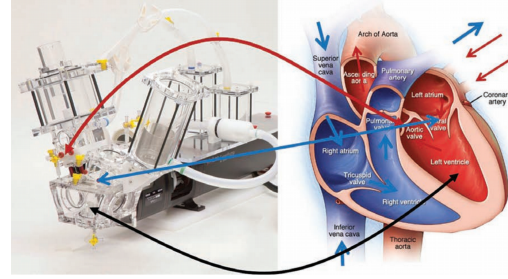
Figure 5. Pulse Duplicator device (left) and schematic of the heart anatomy (right). Arrows show how each chamber of the device represents different parts of the heart, modeling the performance of the left side of the heart. The left chamber of the device is where the BHVs are mounted (as aortic valves) and tested, and where the data are collected. Image from ViVitro Labs Inc.

in diameter, while the third was 19 mm (BHV-3). Two different test sessions were recorded for BHV-2, at 50 million cycles and at 200 million cycles. The dataset thus comprises four different experimental cases with videos and the associated pressure and flow data: "BHV-1", "BHV-2-50", "BHV-2-200", and "BHV-3".

3.2. Numerical Setup

The computational domain is based on the Pulse Duplicator device with some simplifications. It includes a dynamic valve placed inside a 3D cylinder (Figure 6a). To emulate a valve as genuinely as possible, the geometrical evolution of the valve orifice is taken directly from the real cases (not modeled). Since the only source for that information comes from the 2D camera imagery data providing projection of the actual 3D valve on the x-y plane, we simulate a 2D valve on the x-y plane perpendicular to the flow direction. Although this simplification may affect the flow pattern, the overall flow symmetries (and asymmetries) are expected to be reproduced. For each valve, we also simulate an equivalent ideal valve, with the orifice area equal to that of the actual valve but with a circular shape opening, providing an ideal symmetry. The results of those equivalent valves are used to remove the trends that are valve-independent (e.g. boundary condition effects). The working fluid is saline with a density of $\rho = 1000$ kg/m^3 and a viscosity of $\mu = 0.001$ Pa s. The boundary conditions include the measured velocity and pressure at the inlet and outlet, respectively (Figure 6b). The domain is represented with a particle (node) size of $d_p = 0.035d$, where d is the valve diameter ($d = 25$ mm in Figure 6c, resulting in around 125,000 particles). A sensitivity analysis with respect to the particle size shows that smaller particle sizes would have an insignificant impact on the results. The time step size is automatically determined by the model to guarantee a stable solution. Figure 7 shows example flow simulations through a valve at two different moments in the cardiac cycle, including snapshots of the simulation results (streamwise ve-
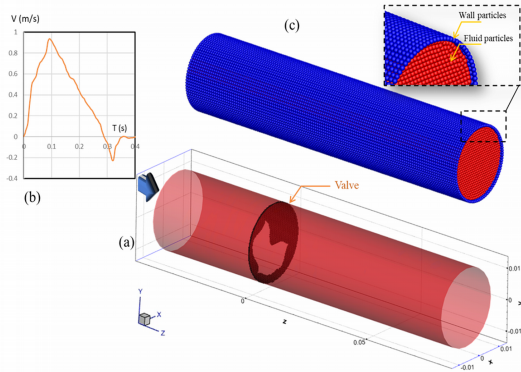
Figure 6. Numerical setup: (a) computational domain for a valve with a 25 mm diameter, (b) inlet boundary condition, i.e. known velocity time series, and (c) particle representation of the computational domain. The "Valve" tag indicates the profile of the orifice, obtained from the high-quality video.
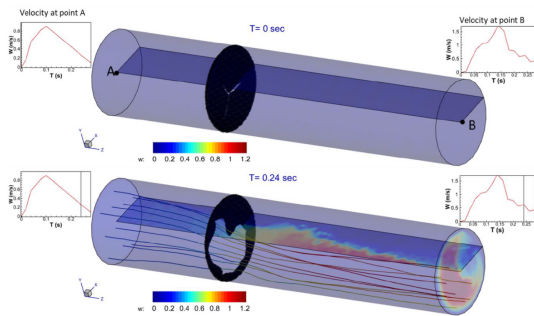
Figure 7. Example flow simulations through a valve, with a snapshot of the simulation results (streamwise velocity component w, and streamline), and velocity time series in two points (A and B).

locity component w, and streamline), and velocity time series at two example points.

3.3. Evaluation

Figure 8 shows the calculated pair-wise leaflet symmetry DOPM and DTW score profiles along with the simulated velocity and vorticity profiles for all four experimental cases. Qualitatively speaking, it is easy to see that the DTW score profiles (second column) are closer to the velocity (third column) and vorticity (fourth column) profiles than the DOPM score profiles (first column). Indeed, except for the BHV-1 case, the global trend of the DOPM score profiles do not appear to follow that of the velocity and vorticity profiles. One possible explanation is that the DOPM score is computed locally, fragment by fragment, and summarized via averaging, whereas the DTW score is computed globally, which may be more appropriate in our case. We can see that the DTW score profiles' ranking of the symmetry among the three leaflet pairs generally follows that found in the velocity and vorticity profiles. For instance, for BHV-1, the $A\&C$ leaflet pair (in blue) is more

Case	Leaflet Pair	DOPM-Velocity	DOPM-Vorticity	DTW-Velocity	DTW-Vorticity
BHV-1	A&B	0.1642	0.1769	0.1288	0.2669
	A&C	0.3186	0.4497	0.1678	0.4525
	B&C	0.2067	0.1596	0.1044	0.2095
BHV-2-50	A&B	0.9252	0.9622	0.2258	0.2663
	A&C	0.9696	1.0321	0.1713	0.1576
	B&C	0.4825	0.5371	0.2510	0.1603
BHV-2-200	A&B	0.4533	0.5153	0.2152	0.2591
	A&C	0.8917	1.0330	0.2995	0.3412
	B&C	0.7257	0.6958	0.2024	0.1863
BHV-3	A&B	0.6383	0.5755	0.2261	0.0899
	A&C	1.1504	1.1040	0.2322	0.0915
	B&C	0.7252	0.6761	0.1932	0.1003
Average		0.6376	0.6598	0.2015	0.2151

Table 1. RSME values of the calculated DOPM and DTW symmetry scores with respect to the simulated velocity and vorticity parameters for all four experimental cases.

visually symmetric than the other pairs, as is shown from the lower values in the DTW, velocity, and vorticity profiles; for BHV-2-50, this is seen for the $B\&C$ leaflet pair (in yellow), etc. The peaks in the DTW profiles generally correspond to the peaks in the velocity and vorticity profiles, e.g. around 15 ms and 280 ms for BHV-3. We can deduce from the DTW score profiles which leaflets cause asymmetries in the valve motion: for instance, looking at BHV-1 (first row, second column), leaflet B is common to the two pairs involved in the largest scores, thus responsible for most asymmetries, which is confirmed by the $A\&C$ pair having the lowest score.

Figure 9 shows the DTW score profile for BHV-2-50 augmented with video frames and the corresponding valve orifice region mask at three key locations of the cardiac cycle. The scores are lower (more symmetry) when the valve is open, and higher (less symmetry) when the valve is opening and closing, as corroborated by the frames.

Table 1 quantitatively compares the graphs of Figure 8. Lower RMSE values are preferable, with 0 indicating a perfect similarity of the graphs. On average, the RMSE values involving DTW are lower than those involving DOPM, which supports our observations on Figure 8. Regarding DOPM, BHV-1 yields the lowest RMSE values, which are comparable to those related to DTW. For the other cases, error values are too high for DOPM to be a reliable symmetry indicator. Regarding DTW, BHV-1 yields the lowest RMSE values for DTW-Velocity, whereas BHV-3 is showing the lowest error for DTW-Vorticity. Overall, DTW serves as a good indicator of valve functional symmetry due to its low error values, as low as 0.0899.

4. Conclusion

This paper shows that the visual symmetry of BHV leaflets is highly correlated with the functional symmetry of the valves. Visual reflection symmetry information, derived from the shape of pair-wise valve leaflet motion, is obtained from video data, acquired during pulsatile flow
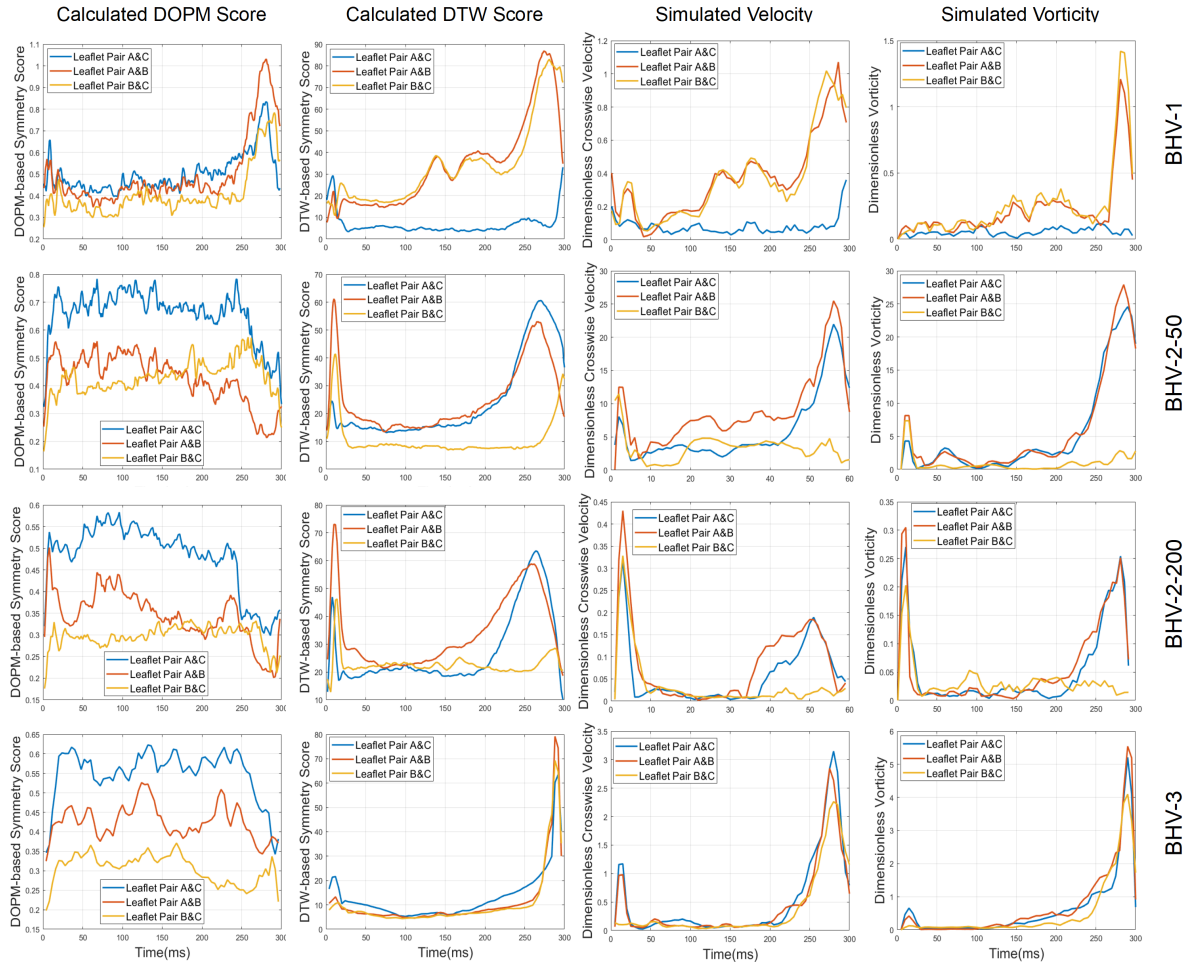
Figure 8. Calculated DOPM and DTW symmetry scores and simulated velocity and vorticity parameters for all four experimental cases.
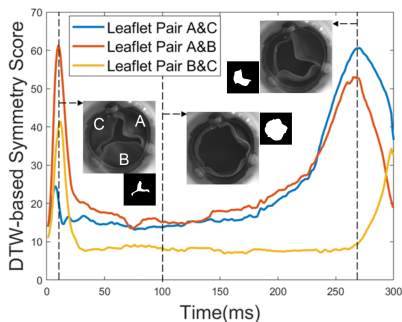
Figure 9. Calculated DTW symmetry score for BHV-2-50, showing frames from the high-quality video and the corresponding valve orifice region mask at three key locations of the cardiac cycle, from left to right: opening, open, and closing phases.

tests, via two different symmetry scores: DOPM and DTW. Functional symmetry information, related to physical values such as velocity and vorticity, is obtained via numerical simulations of the cardiac cycle, using actual data from pulsatile flow tests for the boundary conditions and effective valve orifice area. Experiments on four different cases

that include three tricuspid BHVs of various diameters have shown that DTW score profiles are similar to the profiles of the velocity and vorticity at the leaflet borders, much more so than DOPM profiles. With RMSE values as low as 0.09, the DTW score constitutes a good indicator of the functional symmetry of the valve. This paves the way towards BHV durability estimations based on computer vision methods via symmetry analyses of the leaflet motion. Future research will look at expanding the dataset to cover additional BHV designs, developing a unified symmetry measuring parameter that would allow us to easily compare valves with different video characteristics (frame rates, resolution, etc.), gathering real-world (non-simulated) durability data, and utilizing DTW scores and/or a new unified symmetry parameter to train deep learning networks to estimate BHV design durability based on visual symmetry.

Acknowledgments

References

[1] M. Alizadeh, M. Cote, and A. Branzan Albu. Leaflet free edge detection for the automatic analysis of prosthetic heart valve opening and closing motion patterns from high speed video recordings. In *Scandinavian Conference on Image Analysis (SCIA'17)*, pages 15–27. Springer, 2017.

[2] M. Alizadeh, M. Cote, and A. Branzan Albu. Automatic segmentation and tracking of biological prosthetic heart valves. *Journal of Medical Imaging*, 8(1):015501, 2021.

[3] I. Atadjanov and S. Lee. Bilateral symmetry detection based on scale invariant structure feature. In *IEEE International Conference on Image Processing (ICIP'15)*, pages 3447–3451. IEEE, 2015.

[4] A. Burden, M. Cote, and A. Branzan Albu. Fast and accurate tracking of highly deformable heart valves with locally constrained level sets. In *14th Conference on Computer and Robot Vision (CRV'17)*, pages 109–116. IEEE, 2017.

[5] M. Cho and K.M. Lee. Bilateral symmetry detection via symmetry-growing. In *British Machine Vision Conference (BMVC'09)*, pages 1–11. Citeseer, 2009.

[6] C.R. Choi and C.N. Kim. Numerical analysis on the hemodynamics and leaflet dynamics in a bileaflet mechanical heart valve using a fluid-structure interaction method. *ASAIO Journal*, 55(5):428–437, 2009.

[7] A.P. Condurache, T. Hahn, U.G. Hofmann, M. Scharfschwerdt, M. Misfeld, and T. Aach. Automatic measuring of quality criteria for heart valves. In *Medical Imaging 2007: Image Processing*, volume 6512, page 65122Q. International Society for Optics and Photonics, 2007.

[8] A.P. Condurache, T. Hahn, M. Scharfschwerdt, A. Mertins, and T. Aach. Video-based measuring of quality parameters for tricuspid xenograft heart valve implants. *IEEE Transactions on Biomedical Engineering*, 56(12):2868–2878, 2008.

[9] S. Derrode and F. Ghorbel. Shape analysis and symmetry detection in gray-level objects using the analytical fourier–mellin representation. *Signal Processing*, 84(1):25–39, 2004.

[10] A. Efrat, Q. Fan, and S. Venkatasubramanian. Curve matching, time warping, and light fields: New algorithms for computing similarity between curves. *Journal of Mathematical Imaging and Vision*, 27(3):203–216, 2007.

[11] O. Gold and M. Sharir. Dynamic time warping and geometric edit distance: Breaking the quadratic barrier. *ACM Transactions on Algorithms (TALG)*, 14(4):1–17, 2018.

[12] M. Grigioni, C. Daniele, G. D'Avenio, U. Morbiducci, C. Del Gaudio, M. Abbate, and D. Di Meo. Innovative technologies for the assessment of cardiovascular medical devices: state-of-the-art techniques for artificial heart valve testing. *Expert Review of Medical Devices*, 1(1):81–93, 2004.

[13] T. Hahn, A.P. Condurache, T. Aach, M. Scharfschwerdt, and M. Misfeld. Automatic in-vitro orifice area determination and fluttering analysis for tricuspid heart valves. In *Bildverarbeitung für die Medizin 2006*, pages 21–25. Springer, 2006.

[14] ViVitro Labs Inc. Information about our Pulse Duplicator System. http://vivitrolabs.com/product/pulse-duplicator/. Accessed: 2021-08-11.

[15] M. Jandaghian, A. Krimi, A.R. Zarrati, and A. Shakibaeinia. Enhanced weakly-compressible mps method for violent free-surface flows: Role of particle regularization techniques. *Journal of Computational Physics*, 434:110202, 2021.

[16] S. Kondra, A. Petrosino, and S. Iodice. Multi-scale kernel operators for reflection and rotation symmetry: further achievements. In *IEEE Conference on Computer Vision and Pattern Recognition Workshops (CVPRW'13)*, pages 217–222, 2013.

[17] M. Kondruweit, S. Friedl, C. Heim, T. Wittenberg, M. Weyand, and F. Harig. A new ex vivo beating heart model to investigate the application of heart valve performance tools with a high-speed camera. *ASAIO Journal*, 60(1):38–43, 2014.

[18] M. Kondruweit, S. Friedl, T. Wittenberg, R. Tandler, and M. Weyand. Description of a novel ex-vivo imaging and investigation technique to record, analyze and visualize heart valve motions under physiological conditions. *Heart, Lung and Circulation*, 19:S174, 2010.

[19] K.Y.C. Li. Bioprosthetic heart valves: upgrading a 50-year old technology. *Frontiers in Cardiovascular Medicine*, 6:47, 2019.

[20] N. Lila, C.G.A. McGregor, S. Carpentier, J. Rancic, G.W. Byrne, and A. Carpentier. Gal knockout pig pericardium: new source of material for heart valve bioprostheses. *The Journal of Heart and Lung Transplantation*, 29(5):538–543, 2010.

[21] Y. Liu, H. Hel-Or, C.S. Kaplan, and L. Van Gool. *Computational symmetry in computer vision and computer graphics*. Now Publishers Inc, 2010.

[22] G. Loy and J.-O. Eklundh. Detecting symmetry and symmetric constellations of features. In *European Conference on Computer Vision (ECCV'06)*, pages 508–521. Springer, 2006.

[23] H. Mohammadi and K. Mequanint. Prosthetic aortic heart valves: modeling and design. *Medical Engineering & Physics*, 33(2):131–147, 2011.

[24] Y.S. Morsi, I.E. Birchall, and F.L. Rosenfeldt. Artificial aortic valves: an overview. *The International Journal of Artificial Organs*, 27(6):445–451, 2004.

[25] A. Myronenko and X. Song. Intensity-based image registration by minimizing residual complexity. *IEEE Transactions on Medical Imaging*, 29(11):1882–1891, 2010.

[26] V. Patraucean, R. Grompone von Gioi, and M. Ovsjanikov. Detection of mirror-symmetric image patches. In *IEEE Conference on Computer Vision and Pattern Recognition Workshops (CVPRW'13)*, pages 211–216, 2013.

[27] D. Reisfeld and Y. Yeshurun. Robust detection of facial features by generalized symmetry. In *International Conference on Pattern Recognition (ICPR'92)*, pages 117–117. IEEE COMPUTER SOCIETY PRESS, 1992.

[28] A. Roche and N. Malandain, G.and Ayache. Unifying maximum likelihood approaches in medical image registration. *International Journal of Imaging Systems and Technology*, 11(1):71–80, 2000.

[29] A. Shakibaeinia and Y.-C. Jin. A weakly compressible mps method for modeling of open-boundary free-surface flow. *International Journal for Numerical Methods in Fluids*, 63(10):1208–1232, 2010.

[30] D. Shen, H.H.S. Ip, K.K.T. Cheung, and E.K. Teoh. Symmetry detection by generalized complex (gc) moments: a close-form solution. *IEEE Transactions on Pattern Analysis and Machine Intelligence*, 21(5):466–476, 1999.

[31] R.F. Siddiqui, J.R. Abraham, and J. Butany. Bioprosthetic heart valves: modes of failure. *Histopathology*, 55(2):135–144, 2009.

[32] I. Vesely. The evolution of bioprosthetic heart valve design and its impact on durability. *Cardiovascular Pathology*, 12(5):277–286, 2003.

[33] Z. Wang, M. Liang, and Y.F. Li. Using diagonals of orthogonal projection matrices for affine invariant contour matching. *Image and Vision Computing*, 29(10):681–692, 2011.

[34] Z. Wang, Z. Tang, and X. Zhang. Reflection symmetry detection using locally affine invariant edge correspondence. *IEEE Transactions on Image Processing*, 24(4):1297–1301, 2015.

[35] H. Weyl. *Symmetry*. Princeton University Press, 2015.

[36] T. Wittenberg, R. Cesnjevar, S. Rupp, M. Weyand, and M. Kondruweit. High-speed-camera recordings and image sequence analysis of moving heart-valves: experiments and first results. In *Advances in Medical Engineering*, pages 169–174. Springer, 2007.

[37] P. Zilla, J. Brink, P. Human, and D. Bezuidenhout. Prosthetic heart valves: catering for the few. *Biomaterials*, 29(4):385–406, 2008.